# The H–NCS bond energy, $\Delta H_f^\circ$ (HNCS), $\Delta H_f^\circ$ (NCS), and IP(NCS) from photoionization mass spectrometric studies of HNCS, NCS, and $(NCS)_2$

B. Ruscic and J. Berkowitz
*Chemistry Division, Argonne National Laboratory, Argonne, Illinois 60439*

(Received 2 May 1994; accepted 27 July 1994)

The species HNCS and NCS have been studied by photoionization mass spectroscopy. The adiabatic ionization potential (IP) of HNCS is $\leqslant$9.92 eV; the shape of the ion yield curve near threshold implies a large change in geometry, perhaps to linear $HNCS^+$. Various appearance potentials (AP) from HNCS are determined by a more objective procedure, from which $\Delta H_f^\circ$(HNCS)>29.6 kcal/mol (and very likely $\geqslant$31.0±0.7 kcal/mol) is deduced. The adiabatic IP of NCS is 10.689±0.005 eV. This quantity, together with AP($NCS^+$/HNCS), yields $D_0$(H–NCS)$\leqslant$97.2±0.2 kcal/mol. However, a measurement of the appearance potential of $NCS^+$ from $(NCS)_2$ results in a still lower value, $D_0$(H–NCS)$\leqslant$93.3±1.1 kcal/mol, and $\Delta H_{f_0}^\circ$(NCS) $\leqslant$ 72.7 ± 0.8 kcal/mol. Approximate values are obtained for $\Delta H_{f_0}^\circ$($HNCS^+$) and for the proton affinity of NCS.

## I. INTRODUCTION

Recently, a great deal of attention has been directed at determining the structures and relative stabilities of the CHNO isomers,[1] but much less is known about the CHNS isomers. In Fig. 1, we compare the structures and relative stabilities of the CHNO isomers, calculated by several groups[2–5] in the past two years, with calculations on the CHNS isomers reported[6] in 1977. In both CHNO and CHNS, the electronic ground state has the form HNCY (Y=O, S), and is referred to as isocyanic (isothiocyanic) acid. These species can be prepared readily, and have been subjected to extensive spectroscopic study. The lowest excited isomers (NCYH), involving the migration of H to the other end of the NCY radical, are called cyanic (thiocyanic) acid and have heretofore not been isolated in the gas phase. In the more highly excited isomers, there is an apparent reversal between the oxy and thioforms, with HCNO (fulminic acid) having a lower energy than CNOH (isofulminic acid), whereas CNSH has a lower calculated energy than HCNS. Of these excited isomers, only HCNO has been prepared and studied spectroscopically in the gas phase. Figure 1 shows that corresponding oxy and thio isomers have similar structures. Also, the excitation energies of the thio isomers appear to be substantially smaller than those of the oxy isomers.

Experimental studies have established the structures of HNCO, HCNO, and HNCS from microwave spectra, and the vibrational frequencies of these species are also known. Recently, there has been some uncertainty regarding the heats of formation of HNCO and NCO and the corresponding bond energy, which is nearing resolution.[1] For HNCS, this issue is just now being joined. The experimental determination of $\Delta H_f^\circ$(HNCO) is based upon the measured photodissociative threshold[7] for the formation of NH($a\ ^1\Delta$) and CO. By contrast, the currently listed[8] value for the heat of formation of HNCS has a rather different genesis. The value listed by Lias *et al.*[8] [$\Delta H_{f298}^\circ$(HNCS)=31 kcal/mol] is copied from the earlier NBS compilation by Wagman *et al.*[9] $\Delta H_{f298}^\circ$(HNCS)=30.5 kcal/mol, without a source reference. The current NIST records[10] reveal that it is based on a heat of solution of ammonium thiocyanate determined[11] in 1882 and an enthalpy of vaporization of cyanic acid solutions obtained by Brandenburg[12] in 1958 in an otherwise unpublished Ph.D. thesis. Domalski[10] believes that the listed value may be accurate to ±1.5 kcal/mol.

The closest analog to the photodissociation threshold method [applied to measuring $\Delta H_f^\circ$(HNCO)] for inferring $\Delta H_f^\circ$(HNCO) was a study by Lenzi *et al.*[13] These authors observed fluorescence from CS($A\ ^1\Pi$) upon irradiating HNCS with vacuum ultraviolet light, according to the reactions

$$HNCS + h\nu \rightarrow NH(X\ ^3\Sigma^-) + CS(A\ ^1\Pi), \quad (1)$$

$$CS(A\ ^1\Pi) \rightarrow CS(X\ ^1\Sigma^+) + h\nu. \quad (2)$$

Using line sources, they observed fluorescence at a Kr resonance line (1165 Å≡10.64 eV), but did not observe it at H Lyman-$\alpha$, 1215.7 Å≡10.20 eV.[14] At the time, Lenzi *et al.* did not have available to them accurate values of $\Delta H_f^\circ$(NH) and $\Delta H_f^\circ$(CS). Hence, they used the NBS value for $\Delta H_f^\circ$(HNCS) to infer appropriate values for the product heats of formation which, from currently available knowledge, were too high for both NH and CS. With the best current information [$\Delta H_{f_0}^\circ$(NH)=85.5±0.3 kcal/mol,[15] $\Delta H_{f_0}^\circ$(CS)=65.8±0.6 kcal/mol,[16] $h\nu$=38 797.6 $cm^{-1}$ [17] in Eq. (2)] and a photodissociative threshold $\geqslant$10.20 eV, we can infer $\Delta H_f^\circ$(HNCS) $\leqslant$27.3±0.7 kcal/mol. Here, we have intentionally not specified whether this evaluation refers to 298 or 0 K. Thus, if we take the observations of Lenzi *et al.* at face value, there appears to be a discrepancy of ~3 kcal/mol between the inference from photodissociative thresholds and the tabulated value for $\Delta H_f^\circ$(HNCS).

Let us now consider an alternative dissociation,

$$HNCS \rightarrow H + NCS. \quad (3)$$

Then,

$$\Delta H_f^\circ(HNCS) = \Delta H_f^\circ(H) + \Delta H_f^\circ(NCS) - D_0(H\text{–}NCS). \quad (4)$$

Bradforth *et al.*[18] have recently determined an accurate value of the electron affinity of NCS (3.537±0.005 eV and combined it with a gas phase acidity for HNCS[8] to deduce

 0021-9606/94/101(9)/7975/15/$6.00  

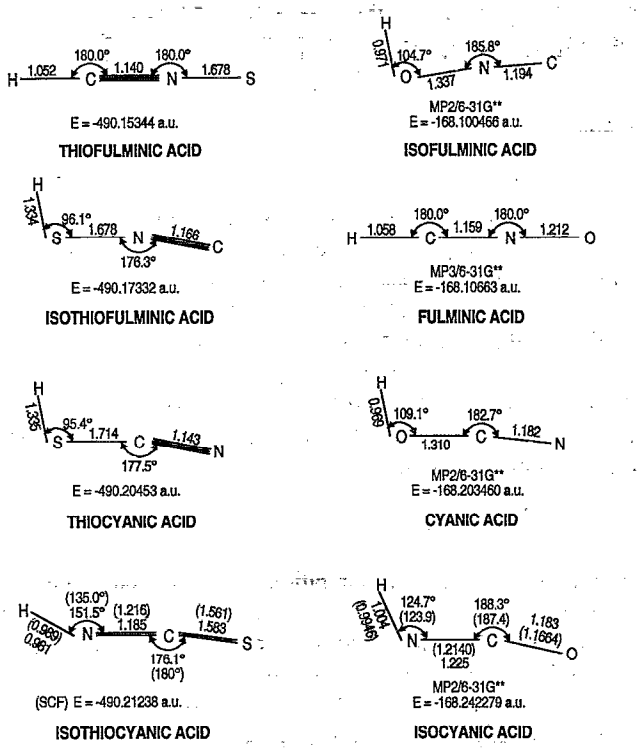


FIG. 1. Comparison of *ab initio* calculated structures and energies for the CHNS isomers (from Ref. 6) and the CHNO isomers [from J. H. Teles, G. Maier, B. A. Hess, Jr., L. J. Schaad, M. Winnewisser, and B. P. Winnewisser, Chem. Ber. **122**, 753 (1989)]. Slightly different structures and energies for HNCS and HSCN are given in Ref. 28. For the meaning of the numbers in parentheses, see Ref. 6 and Teles *et al.* 1 a.u.=627.5 kcal/mol.

$D_{298}$(H–NCS)=96±6 kcal/mol. (Our examination[19] of this gas phase acidity gives 95.4±5 kcal/mol.) An earlier determination of $\Delta H_f^\circ$(NCS) had been made by D'Amario *et al.*[20] who measured the onset of $A \rightarrow X$ emission from NCS following the photodissociation of $CH_3NCS$ and $CH_3SCN$. They deduced $\Delta H_f^\circ$(NCS)=76.4±1 kcal/mol from their reported thresholds. However, several problems attend their evaluation. The $A-X$ excitation energy is now 3.245 eV,[21] whereas they used 3.26 eV. Their utilized value for $\Delta H_f^\circ(CH_3)$ was 33.2 kcal/mol, whereas the current values are $\Delta H_{f_0}^\circ(CH_3)$=35.8±0.1 kcal/mol and $\Delta H_{f298}^\circ(CH_3)$ =35.0±0.1 kcal/mol. No effort was made to take into account the initial internal energy of $CH_3NCS$ or $CH_3SCN$, and indeed, it is not clear whether the derived $\Delta H_f^\circ$(NCS) refers to 298 or 0 K. Also, the chosen thresholds for fluorescence appeared to be well into the tail region. Tokue *et al.*[22] repeated these measurements more recently. They observed almost the same threshold for photodissociation of $CH_3NCS$ (188.8±1.0 nm vs 188±1 nm), but a rather different threshold for photodissociation of $CH_3SCN$ (193.2±1.0 nm vs 198±1 nm). If we use more modern values for the $A-X$ excitation energy and $\Delta H_f^\circ(CH_3)$ and treat these thresholds with and without internal excitation energy, the resulting values of $\Delta H_{f_0}^\circ$(NCS) range from 74.2 to 79.7 kcal/mol.

The approach we shall adopt here is to measure photodissociative ionization thresholds from HNCS. Many processes are possible, including $S^+$+HCN(HNC), $HCS^+$+N, $SH^+$+CN, $NS^+$+CH, $CS^+$+NH and the corresponding reactions in which the charge appears on the other partner, which should occur at higher energy and are less likely. The heats of formation of the products are rather well-known. If we combine them with the tabulated value of $\Delta H_f^\circ$(HNCS), we can predict the anticipated onsets for these processes. These values are listed in Table I. If we can establish more accurate thresholds, we shall be in a position to deduce a more accurate value for $\Delta H_f^\circ$(HNCS).

Not listed in Table I is the anticipated appearance potential for $NCS^+$+H. This value depends upon the ionization potential of NCS about which nothing is known, and $\Delta H_f^\circ$(NCS). If we can determine the appearance potential of $NCS^+$(HNCS), and independently the ionization potential of NCS, we can establish an upper limit to $D_0$(H–NCS). In order to test the accuracy of this upper limit, it is desirable to examine at least one other molecule which will also dissociatively ionize to form $NCS^+$. An attractive candidate is thiocyanogen, NCS–SCN. Its heat of formation is independently known, and one can surmise that a low-energy dissociative ionization process will yield $NCS^+$+NCS. Thus, if the ionization potential of NCS can be established, the threshold for $NCS^+$ from thiocyanogen yields an alternative upper limit for $\Delta H_f^\circ$(NCS), and hence $D_0$(H–NCS). Since NCS appears twice as a product, the uncertainty in $\Delta H_f^\circ$(NCS) from this latter measurement is roughly half the combined uncertainty in the measured appearance potential and $\Delta H_f^\circ$(NCS–SCN).

A perusal of Table I indicates that problems may be encountered with the planned study of HNCS. Process 2, the lowest energy dissociative ionization reaction, is usually the most reliable. However, it is clear that rearrangement must occur to form HCN, and not HNC, as the neutral partner. This implies a "tight" transition state for this reaction, which could lead to a delayed onset. Process 3, forming $HCS^+$, also requires a rearrangement. In the analogous study of HNCO, it was found that $HCO^+$ had a much higher appearance potential than anticipated, and was useless for thermochemical purposes. Rearrangement is also necessary for processes 4 and 7. Process 5 does not require rearrangement, but is less likely since there will be a preference for the charge to appear on the partner, S atom. In addition, $\Delta H_f^\circ(HNC^+)$ is not well-established. One must await process 6 before simple bond cleavage appears. This analysis does not include the process $NCS^+$+H (which is a simple cleavage) whose anticipated appearance potential awaits our determination of IP(NCS), *vide infra*.

## II. EXPERIMENTAL ARRANGEMENT

The basic apparatus consisting of a tunable VUV light source, an ionization region where molecular source and selected radiation intersect, and a mass spectrometer to identify the ions of interest has been described previously.[23] The bandwidth of the 3 m VUV monochromator for these experiments was 0.84 Å (FWHM). Isothiocyanic acid was prepared by adding dropwise a saturated solution of KSCN to a bulb containing 90%–95% solution of phosphoric acid on a vacuum line. Nitrogen was bubbled through the mixture,

TABLE I. Ionization and anticipated appearance potentials from HNCS, based on available thermochemical data[a] prior to the present research.

| No. | Process | Appearance energy (eV)[b] | Reference |
|---|---|---|---|
| 1. | $HNCS+h\nu \rightarrow HNCS^+ + e$ | 10.05±0.1 | Ref. 25 |
| | | 9.94±0.02 | Ref. 26 |
| 2. | $\rightarrow S^+ + HCN$ | 13.20±0.07 | $\Delta H_f^\circ(S)$ from Ref. 41, IP(S) from Ref. 42; for $\Delta H_f^\circ(HCN)$ see Ref. 43 |
| 2′. | $\rightarrow S^+ + HNC$ | 13.84±0.11 | $\Delta H_f^\circ(HNC)=\Delta H_f^\circ(HCN)+14.8(\pm 2)$ kcal/mol from C-F. Pau and W. J. Hehre, J. Chem. Phys. **86**, 321 (1982) |
| 3. | $\rightarrow HCS^+ + N$ | 14.05±0.11 | $\Delta H_f^\circ(HCS^+)=242.6\pm 2.0$ kcal/mol from B. Ruscic and J. Berkowitz, J. Phys. Chem. **98**, 2568 (1993) |
| 4. | $\rightarrow SH^+ + CN$ | 15.06±0.07 | $\Delta H_f^\circ(SH)$ from Ref. 38, IP(SH) from Ref. 39, $\Delta H_{f_0}^\circ(CN)$ from Ref. 40 |
| 5. | $\rightarrow HNC^+ + S$ | 16.07±0.12 | $\Delta H_f^\circ(HNC^+)=$(336 kcal/mol) from Ref. 8 |
| 6. | $\rightarrow CS^+ + NH$ | 16.55±0.07 | For $\Delta H_{f_0}^\circ(NH)$, see Ref. 15, for $\Delta H_{f_0}^\circ(CS)$, see Ref. 16, for IP (CS), see Ref. 17 |
| 7. | $\rightarrow NS^+ + CH$ | 16.71±0.11 | $\Delta H_f^\circ(NS)=70\pm 2$ kcal/mol inferred from $D_0(NS)=108.2\pm 2$ kcal/mol from L. A. Curtiss, K. Raghavachari, G. W. Trucks, and J. A. Pople, J. Chem. Phys. **94**, 7221 (1991) IP(NS)=8.87±0.01 eV from J. M. Dyke, A. Morris, and I. R. Trickle, J. Chem. Soc. Faraday Trans. II **73**, 147 (1977) |
| 8. | $\rightarrow NH^+ + CS$ | 18.69±0.07 | For $\Delta H_{f_0}^\circ(NH^+)$, see Ref. 15; for $\Delta H_{f_0}^\circ(CS)$, see Ref. 16 |

[a]We assume here $\Delta H_{f_0}^\circ(HNCS) = 31.1 \pm 1.5$ kcal/mol, based on $\Delta H_{f_{298}}^\circ(HNCS) = 30.5 \pm 1.5$ kcal/mol given in Ref. 9. Other values are form Ref. 41, except where noted.
[b]The error bars in the appearance energies reflect the uncertainties in the heats of formation of the products, but not that of HNCS.

which was kept at −16 °C and stirred. The entrained HNCS gas, plus other volatile impurities were condensed in a liquid nitrogen trap. After the reaction was completed, a dry-ice trap was substituted for the liquid $N_2$ trap, and the condensate was pumped upon for several hours, to remove more volatile impurities. The product was introduced into the apparatus at dry ice temperature, or in some cases at −16 °C. The NCS transient species was prepared *in situ* by the reaction of F atoms (generated in a microwave discharge through $F_2$) with HNCS. Thiocyanogen was prepared by passing $Cl_2$ over dry AgSCN supported on glass wool, as described by Frost *et al.*[24]

## III. EXPERIMENTAL RESULTS

### A. Photoionization of HNCS

#### 1. Overview

The mass spectrum of HNCS observed at 584 Å=21.2 eV is listed in Table II. These relative intensities must be considered qualitative, as no correction was applied for the mass discrimination of the quadrupole mass spectrometer, nor for discrimination due to fragment kinetic energies. In addition, some impurities (mostly COS) were present, but (except for $HCN^+$) these are not expected to influence the thresholds nor the photoion yield curves of the major fragments from HNCS. The parent ion is clearly the most intense, followed by the fragment ions $S^+$, $NCS^+$, $HCN^+/HNC^+$, and $SH^+$. All other peaks originating from HNCS have an abundance <1% of $HNCS^+$. The abundance of fragment ions generally follows the anticipated intensities based on the calculated appearance potentials given in Table I, except for $HCS^+$, which is weaker but presumably is consequent upon a major rearrangement, and $HCN^+$, which is stronger and was subsequently identified as due to HCN impurity.

An overview of the photoion yield curves of the major

TABLE II. Photoionization mass spectrum[a] of HNCS at 584 Å=21.2 eV.

| *m/e* | Species | Relative intensity |
|---|---|---|
| 60 | Mostly $COS^+$ (impurity) | 27.0 |
| 59 | $HNCS^+$ | 100.0 |
| 58 | $NCS^+$ | 12.9 |
| 46 | $NS^+$ | 0.6 |
| 45 | $HCS^+$ | 0.8 |
| 44 | $CS^+$ | 0.7 |
| 33 | $SH^+$ | 2.5 |
| 32 | $S^+$ | 37.3 |
| 28 | $CO^+$ (impurity) | 1.6 |
| 27 | $HCN^+/HNC^+$ | 5.5 |
| 26 | $CN^+$ | 0.2 |
| 15 | $NH^+$ | ~0.03 |
| 13 | $CH^+$ | ~0.01 |

[a]The $^{34}S$ contributions appearing at $m/e=61$ and 34 ($HNCS^+$ and $S^+$) are not shown.

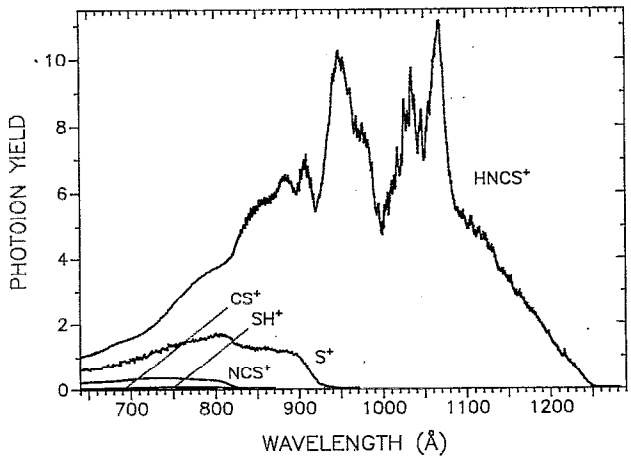


FIG. 2. Overview of the photoion yield curves of the major species from HNCS from the ionization potential to 640 Å. The relative intensities are significant, within the limitations of quadrupole mass and kinetic energy discrimination.

species is displayed in Fig. 2. The relative intensities are meaningful here, when the qualifying statements (*vide supra*) are taken into account. As expected, the $HNCS^+$ intensity dominates throughout the region from the ionization potential to 640 Å (and presumably to 584 Å). Pronounced autoionizing structure can be seen in the parent ion, and is discussed below. In addition, the threshold behavior of $HNCS^+$, $S^+$, $NCS^+$, $SH^+$, and $CS^+$ (seen in Fig. 2) and the still weaker $NS^+$, will be analyzed.

### 2. $HNCS^+$

The photoion yield curve of $HNCS^+$(HNCS) bears little resemblance to that of $HNCO^+$(HNCO),[1] and also is difficult to relate to the He I photoelectron spectrum.[24] It is best discussed in terms of (a) the threshold region and (b) the autoionizing region.

*a. Threshold region.* Eland[25] initially presented the He I photoelectron spectra of HNCO and HNCS, and related both to the photoelectron spectrum of the isoelectronic $CO_2$. In the latter, the first photoelectron band is sharp, characterizing photoelectron ejection from the nonbonding or slightly antibonding HOMO, a $\pi_g$ orbital. This orbital is split in the nonlinear HNCO and HNCS into $a'$ (in-plane) and $a''$ (out-of-plane). In Eland's model, the $a'$ orbital becomes a lone pair on the nitrogen atom, while the $a''$ orbital retains its $\pi$ character. Ionization from the latter orbital does not affect the HNC bond angle, and hence a sharp photoelectron band is expected, whereas ionization from $a'$ induces a progression in the HNC bending mode in the cation. This pattern is observed in the partially resolved first two bands in the photoelectron spectrum of HNCO, and appears to be in HNCS. Eland notes that "the strong first ionization bands of $CS_2$ and $H_2S$ overlap" the anticipated sharp band in HNCS, but he concludes that "it is nevertheless quite sharp," with an ionization potential of 10.05±0.1 eV (while the second band consists of a long progression of closely spaced peaks with a vertical IP of 10.35±0.1 eV). Cradock *et al.*[26] also obtained the He I photoelectron spectrum of HNCS, and report 9.94 ±0.02 eV for the vertical first ionization potential, and 10.3 ±0.1 eV for the second. They do not display a spectrum, and nothing is said about overlapping impurity bands. In their comprehensive paper covering many molecules, they have chosen to annotate certain bands as nonbonding, i.e., sharp, and others as consisting of progressions. It may be significant that they have designated the first band in HNCO as nonbonding, but not the first band in HNCS.

The photoion yield curve of $HNCS^+$(HNCS) displays a nearly linear increase with decreasing wavelength, from a threshold value of ~1250 Å to about 1140 Å, with perhaps some very weak autoionizing structure superposed. This is indicative of a large change in geometrical structure between HNCS and $HNCS^+$. The structure of HNCS is fairly well-established experimentally.[27] It is planar, with a nearly linear NCS skeleton (the NCS angle is 173.8°) and an HNC angle of 131.7°. *Ab initio* calculations[6,28] have reproduced this structure fairly well. The $HNCS^+$ structure has heretofore not been known. Curtiss[29] has now calculated this structure to be linear. Such a change in geometry could explain our observations. It apparently does not occur in the isovalent molecules HNCO and $HN_3$. Why should it occur for HNCS? The explanation appears to involve the character of the highest occupied molecular orbital (HOMO). In HNCO, this orbital is localized around HNC. According to recent *ab initio* calculations,[30] the ionization potential of HNC is ~11.9 eV. At the oxygen/sulfur end of the molecule, we can compare CO (IP=14.01 eV) and $CO_2$ (IP=13.78 eV) with CS (IP =11.33 eV), COS (IP=11.17 eV), and $CS_2$ (IP=10.06 eV). The IP of HNC is seen to be lower than for the oxygenated species, but higher than for the sulfur-containing species. Thus, the HOMO in HNCS can be expected to be localized near the C–S region, or at least to have a significant contribution from the sulfur atom. According to Curtiss' calculation, electron ejection from this orbital results in an increase in the C–S distance of ~0.1 Å, but a decrease in the C–N distance. This stiffened C–N bond appears to favor a linear H–N–C structure. For the HNC radical, both the neutral species and the cation are linear.[30] However, the neutral species is rather floppy, having a bending frequency of 464 $cm^{-1}$,[31] whereas the corresponding value for the cation is 618 $cm^{-1}$.[30] In addition, the CN distance decreases by 0.03 Å upon ionization, similar to the calculated behavior of HNCS.

Thus, the alteration in geometry for HNCS upon ionization apparently involves a change in HNC angle, N–C distance, and C–S distance, which would correspond to the gradually increasing photoion yield curve between ~1250–1140 Å. On this basis, the adiabatic ionization potential of HNCS is $\geqslant$1250 Å, or $\leqslant$9.92 eV. The curve appears to diminish further, in an exponential fashion, to ~1260 Å, but here it is difficult to distinguish between Boltzmann factors and weak Franck–Condon factors.

*b. The autoionizing region.* A magnified view of the autoionizing region of the photoion yield curve of $HNCS^+$(HNCS) appears in Fig. 3. The more prominent autoionization peaks are listed in Table III. On energetic grounds, we postulate that these peaks are to be assigned to Rydberg

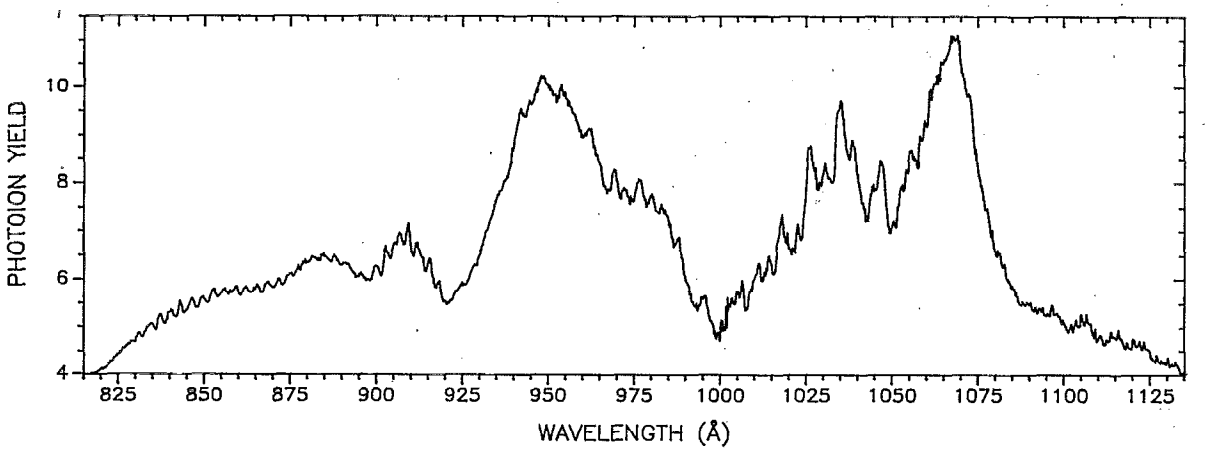


FIG. 3. The autoionizing region of the photoion yield curve of the parent ion from HNCS.

series converging to limits corresponding to Eland's third and fourth photoelectron bands.

We initially focus our attention on the intriguing alternation of intensity of the fine structure in the bands centered at ~1038 and ~980 Å. The average spacing of this fine structure in both bands is about 0.105 eV. Eland notes vibrational structure in the third photoelectron band, with a mean frequency of 856 $cm^{-1}$≡0.106 eV. Cradock *et al.* give 0.105 eV for this spacing. Hence, we shall attempt to relate these autoionizing bands to the limit given by the third photoelectron band. Eland gives the adiabatic IP for this third band as 13.33 ±0.03 eV. With his vibrational spacing, the vertical IP becomes 13.54±0.03 eV. Cradock *et al.* report 13.31±0.02 eV as the vertical IP.

Using the maximum of the band at 1035.0 Å≡11.979 eV and Eland's vertical IP, together with the Rydberg formula

$$E_n = \mathrm{IP} - \frac{R}{(n^*)^2},$$

where $E_n$ is the term value, $R$ the Rydberg constant, and $n^*$ the effective quantum number, we obtain $n^*=2.952$. The next member of this series would then be expected at ~978.6 Å. With the limit given by Cradock *et al.* the 1035 Å feature corresponds to $n^*=3.197$, and the next member should appear at 988.9 Å. It is difficult to determine precisely where this next band in the photoion yield curve has its maximum, since it is contiguous to a still larger band, but it appears to be close to the value inferred from Eland's IP. The 988.9 Å prediction appears to correspond to a region near the onset rather than the maximum of this band. Returning to the limit inferred from Eland, we can predict a still higher Rydberg member ($n^*=4.952$) to occur at ~955 Å. This wavelength is in the region of the maximum of the large contiguous band. There appears to be some vibrational fine structure here, but it is obviously overlapped by another feature.

Continuing to higher energy, we find a band centered at ~909.3 Å≡13.635 eV, with vibrational fine structure having a mean spacing of 0.046 eV≡370 $cm^{-1}$, another broad band with barely visible fine structure centered at ~884.7 Å≡14.014 eV, and then a long vibrational progression between ~875–830 Å, with no obvious maximum, and an average spacing of 0.053 eV≡430 $cm^{-1}$. All of these features have energies beyond the third photoelectron band, and hence presumably converge to the fourth photoelectron band. Eland notes that "part of a progression in 445 $cm^{-1}$ can be made out" in the fourth photoelectron bend. Eland assigns this vibration to the N–H bending mode, but other candidates could be an NCS bend (~370 $cm^{-1}$ in NCS), and a torsional mode (539 $cm^{-1}$ in neutral HNCS). The vertical IP of the fourth band is given by Cradock *et al.* as 15.12±0.02 eV. Eland's paper lists 10.35±0.1 eV, which is obviously a misprint; from his figure, we can extract ~15.24 eV for the vertical IP. With these limits, we can test the bands centered at ~909 and ~885 Å, using the Rydberg formula. The values of $n^*$ obtained are (Eland/Cradock)

909 Å: 2.912/3.027,

885 Å: 3.332/3.508.

Hence, these must be members of different Rydberg series. The next member corresponding to the 909 Å band would occur at ~864 (Eland) or ~868 Å (Cradock). Although the vibrational progression persists throughout this region, there is no obvious maximum. The succedent of the member at 885 Å would occur at ~854 (Eland) or ~858 Å (Cradock). There is a hint of a maximum in the broad region at ~852.6 Å.

The remaining features requiring discussion are the intense, broad features centered at 1068.3 Å≡11.606 eV, and ~950 Å≡13.051 eV. The later may be the antecedent of the 885 Å band, with an $n^*$ value of 2.507/2.579. The former could conceivably be the antecedent of the 909 Å band, with an $n^*$ value of 1.935/1.968, or it could be an isolated member of a series converging to the third photoelectron band, with an $n^*$ of 2.652/2.825.

TABLE III. Wavelengths of the more prominent autoionization peaks appearing in the photoion yield curve of $HNCS^+$(HNCS). b=broad; m=multiple peak; sh=shoulder; ?=uncertain.

| λ (Å) | E (eV) |
|---|---|
| 1132.0 ± 1.0 b,m | $10.95_3 \pm 0.01_0$ |
| 1122.5 ± 1.0 b,m | $11.04_5 \pm 0.01_0$ |
| 1115.0 ± 1.0 b,m | $11.12_0 \pm 0.01_0$ |
| 1110.6 ± 0.5 | 11.164 ± 0.005 |
| 1106.0 ± 1.0 b,m | $11.21_0 \pm 0.01_0$ |
| 1098.0 ± 1.0 b,m | $11.29_2 \pm 0.01_0$ |
| 1081.4 ± 0.5 sh | 11.465 ± 0.005 |
| 1077.6 ± 0.5 sh | 11.506 ± 0.005 |
| 1074.4 ± 0.5 sh,? | 11.540 ± 0.005 |
| 1077.2 ± 0.5 sh | 11.510 ± 0.005 |
| 1068.3 ± 0.7 b,m | 11.606 ± 0.008 |
| 1064.3 ± 0.5 sh | 11.649 ± 0.005 |
| 1063.0 ± 0.5 sh | 11.664 ± 0.005 |
| 1061.0 ± 0.5 | 11.686 ± 0.006 |
| 1059.6 ± 0.5 | 11.701 ± 0.006 |
| 1058.2 ± 0.5 | 11.717 ± 0.006 |
| 1056.5 ± 0.5 sh | 11.735 ± 0.006 |
| 1055.5 ± 0.5 | 11.746 ± 0.006 |
| 1054.0 ± 0.5 sh | 11.763 ± 0.006 |
| 1052.6 ± 0.5 | 11.779 ± 0.006 |
| 1051.8 ± 0.5 sh | 11.788 ± 0.006 |
| 1050.6 ± 0.5 | 11.801 ± 0.006 |
| 1046.7 ± 0.5 | 11.845 ± 0.006 |
| 1044.5 ± 0.5 | 11.870 ± 0.006 |
| 1039.0 ± 0.5 sh | 11.933 ± 0.006 |
| 1038.4 ± 0.5 | 11.940 ± 0.006 |
| 1035.0 ± 0.5 | 11.979 ± 0.006 |
| 1034.2 ± 0.5 sh | 11.988 ± 0.006 |
| 1030.4 ± 0.5 | 12.033 ± 0.006 |
| 1027.6 ± 0.5 sh,? | 12.065 ± 0.006 |
| 1026.1 ± 0.5 | 12.083 ± 0.006 |
| 1022.6 ± 0.5 | 12.124 ± 0.006 |
| 1019.6 ± 0.5 sh,? | 12.160 ± 0.006 |
| 1018.0 ± 0.5 | 12.179 ± 0.006 |
| 1014.2 ± 0.5 | 12.225 ± 0.006 |
| 1011.2 ± 0.5 | 12.261 ± 0.006 |
| 1009.8 ± 0.5 sh | 12.278 ± 0.006 |
| 1006.4 ± 0.5 | 12.320 ± 0.006 |
| 1005.0 ± 0.5 | 12.337 ± 0.006 |
| 1003.4 ± 0.5? | 12.356 ± 0.006 |
| 999.5 ± 0.5? | 12.405 ± 0.006 |
| 997.3 ± 0.5 sh | 12.432 ± 0.006 |
| 995.3 ± 0.5 m | 12.457 ± 0.006 |
| 990.4 ± 0.5 sh | 12.519 ± 0.006 |
| 988.9 ± 0.5 sh | 12.538 ± 0.006 |
| 987.9 ± 0.5 | 12.550 ± 0.006 |
| 984.7 ± 0.5 sh | 12.591 ± 0.006 |
| 983.3 ± 0.7 | 12.609 ± 0.009 |
| 980.0 ± 0.5 | 12.651 ± 0.006 |
| 976.4 ± 0.5 | 12.698 ± 0.006 |
| 972.2 ± 0.5 | 12.753 ± 0.007 |
| 969.1 ± 0.5 | 12.794 ± 0.007 |
| 965.3 ± 0.5 sh,? | 12.844 ± 0.007 |
| 964.3 ± 0.5 sh | 12.857 ± 0.007 |
| 962.3 ± 0.5 | 12.884 ± 0.007 |
| 956.5 ± 0.5 sh,? | 12.962 ± 0.007 |
| 955.5 ± 0.5 sh,? | 12.976 ± 0.007 |
| 954.7 ± 0.5? | 12.987 ± 0.007 |
| 953.6 ± 0.5 | 13.002 ± 0.007 |
| 950.0 ± 0.5 sh,? | 13.051 ± 0.007 |
| 948.3 ± 0.7 | $13.07_4 \pm 0.01_0$ |
| 944.5 ± 0.5 | 13.127 ± 0.007 |
| 941.9 ± 0.5 | 13.163 ± 0.007 |
| 935.5 ± 0.7 sh | $13.25_3 \pm 0.01_0$ |
| 928.5 ± 0.5 sh | 13.353 ± 0.007 |
| 925.0 ± 0.5 | 13.404 ± 0.007 |
| 918.0 ± 0.5 | 13.506 ± 0.007 |
| 915.4 ± 0.5 | 13.544 ± 0.007 |
| 913.4 ± 0.5 sh | 13.574 ± 0.007 |
| 911.7 ± 0.5 | 13.599 ± 0.007 |
| 909.3 ± 0.5 | 13.635 ± 0.007 |
| 906.7 ± 0.5 | 13.674 ± 0.008 |
| 905.5 ± 0.5 | 13.692 ± 0.008 |
| 903.3 ± 0.5 sh,? | 13.726 ± 0.008 |
| 902.6 ± 0.5 | 13.736 ± 0.008 |
| 899.8 ± 0.5 | 13.779 ± 0.008 |
| 895.4 ± 0.5 | 13.847 ± 0.008 |
| 891.0 ± 0.7 | $13.91_5 \pm 0.01_1$ |
| 887.7 ± 0.5 | 13.967 ± 0.008 |
| 884.7 ± 0.5 | 14.014 ± 0.008 |
| 883.2 ± 0.5? | 14.038 ± 0.008 |
| 881.3 ± 0.5 | 14.068 ± 0.008 |
| 879.2 ± 0.5 | 14.102 ± 0.008 |
| 877.3 ± 0.5? | 14.132 ± 0.008 |
| 874.7 ± 0.5 | 14.174 ± 0.008 |
| 871.6 ± 0.5 | 14.225 ± 0.008 |
| 868.2 ± 0.5 | 14.281 ± 0.008 |
| 864.4 ± 0.5? | 14.343 ± 0.008 |
| 865.3 ± 0.5 | 14.328 ± 0.008 |
| 861.9 ± 0.5 | 14.385 ± 0.008 |
| 859.3 ± 0.5 | 14.429 ± 0.008 |
| 857.4 ± 0.5? | 14.460 ± 0.008 |
| 855.6 ± 0.5 | 14.491 ± 0.008 |
| 852.6 ± 0.5 | 14.542 ± 0.009 |
| 849.5 ± 0.5 | 14.595 ± 0.009 |
| 846.4 ± 0.5 | 14.648 ± 0.009 |
| 842.9 ± 0.5 | 14.709 ± 0.009 |
| 840.3 ± 0.5 | 14.755 ± 0.009 |
| 837.1 ± 0.5 | 14.811 ± 0.009 |
| 834.3 ± 0.5 | 14.861 ± 0.009 |
| 831.0 ± 0.5 | 14.920 ± 0.009 |
| 829.9 ± 0.5? | 14.940 ± 0.009 |

### 3. Fragment ions from HNCS

In the present context, the major interest in fragment ions is in their appearance potentials, or fragmentation thresholds. Conventionally, analysis of the threshold regions of fragment photoion yield curves has assumed that they have linear onsets at 0 K, i.e., $I(E)=a(E-E_t)$, where $E_t$ is the appearance potential at 0 K. With this assumption, it can be shown[32] that the influence of initial thermal energy (i.e., if the experiment is carried out at a temperature $T$) is to shift the photoion yield curve to lower energy by the average internal energy of the molecule, and to introduce exponential tailing to still lower energy. Thus, an extrapolation of the linear portion of the experimental curve to the background level, shifted to higher energy by the average internal energy, yields the 0 K threshold. Apart from the assumption that all of the internal energy is available for dissociation, there are two aspects of this procedure which may be questioned.

(i) How general is the assumption of a linear ascent for the 0 K fragment yield curve?

(ii) How much arbitrariness is there in selecting the linear, or quasilinear segment of such a curve?

We have recently made an attempt to respond to the latter two questions more objectively. We separate the problem into an assumed 0 K curve (called a kernel function) and

a well-defined internal energy distribution function. The kernel function is convoluted with the internal energy distribution function, and the result compared with experiment. Various kernel functions can be tested, and an objective least-squares criterion can be employed to select the best kernel function, and hence the best estimate for the 0 K appearance potential. In our prior utilization of the formalism,[33] the internal energy distribution function could be assumed to be primarily due to three external rotations and a nearly free internal rotation, and hence had the simple form

$$P(E-E_0)=\frac{(E-E_0)}{(kT)^2}\,e^{-(E-E_0)/kT},$$

where $E_0$ is a particular value of the photon energy $h\nu_0$. Here, we wish to develop a more general thermal distribution function that includes vibrational, as well as rotational energy.

Haarhoff[34] has provided the formalism for this procedure. If we write

$$P(\epsilon)=\rho\, e^{-E/kT},$$

then we show in the Appendix that for the case of HNCS,

$$\rho=\frac{A}{1+\epsilon}\left[\left(1+\frac{\epsilon}{2}\right)\left(1+\frac{2}{\epsilon}\right)^{\epsilon/2}\right]^{15/2}\left[1-\frac{1}{(1+\epsilon)^2}\right]^{-0.432\,079},$$

where $A$ is a constant, and $\epsilon$ is measured in units of the zero point energy $\epsilon_z$. This is a cumbersome expression to utilize in subsequent convolutions. By numerical analysis, we have fitted this expression between $\epsilon=0$–$1.0$ to the analytical form

$$\rho=\text{const}\;\epsilon^{0.983\,485\,43}e^{3.896\,2067\epsilon},$$

or

$$P(\epsilon)=\text{const}\;\epsilon^{0.983\,485\,43}e^{-15.427\,155\epsilon},$$

using $\epsilon_z=11.449\,218$ kcal/mol for HNCS, and Boltzmann temperature $T=298$ K. The quality of the analytical fit can be judged in several ways.

(1) The most probable energy from the analytical fit is 0.730 kcal/mol; from Haarhoff's cumbersome expression, it is 0.662 kcal/mol.

(2) The average energy from the analytical fit is 1.484 kcal/mol; from known frequencies of HNCS and the three rotational modes, it is 1.303 kcal/mol. The form of the analytical expression is very nearly $E\,e^{-E/kT}$, which is that of a 4-rotor, but with an artificial temperature $T=373.5$ K.

(3) Both the Haarhoff function and the analytically fitted expression were convoluted with a linear kernel function, the former by numerical means. The resulting functions, shown in Fig. 4, are almost indistinguishable.

In the following sections describing the various fragment photoion yields, the fitted analytical expression is convoluted with various kernel functions and compared with the experimental curves to deduce the "best" appearance potentials.

*a. $S^+$ from HNCS.* The lowest energy fragment anticipated from Table I, and actually observed, is $S^+$. The photoion yield curve for this fragment is shown in Fig. 5. One can see a linear segment near threshold, but closer to threshold there is a tail which is larger than expected for the exponential tail due to thermal broadening, as will become more

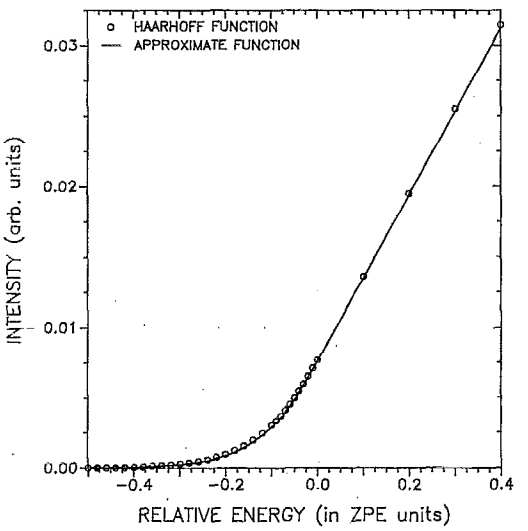


FIG. 4. A comparison of (a) the exact Haarhoff function and (b) an analytically fitted function, both convoluted with a linear kernel function. The abscissa is in units of zero point energy.

apparent later. In addition, the yield increases rather suddenly at ~820 Å≡15.12 eV, which corresponds to the onset of Eland's fourth photoelectron band.

Figure 6 displays the threshold region, and the best fit obtained with a convoluted linear kernel function. One sees that the data points lie above the fitted curve in the tail (13.1–13.4 eV). However, the entire threshold region, including the 0 K threshold intercept at 13.425 eV, lie considerably below the anticipated onset (13.84 eV) for $S^+$+HNC. Consequently, this threshold region must be identified with $S^+$+HCN, which involves some rearrangement from the parent ion structure.

According to Eland, the third photoelectron band has an adiabatic onset at 13.33±0.03 eV. There is a long "Franck–Condon gap" between the end of the second photoelectron

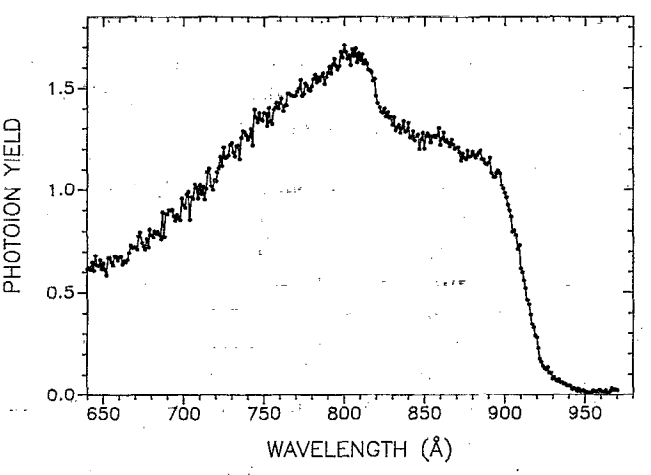


FIG. 5. The photoion yield curve of $S^+$ from HNCS.

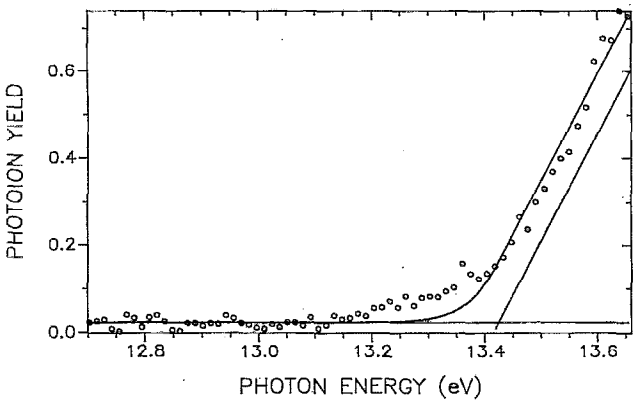


FIG. 6. A magnified view of the threshold region of the photoion yield curve of $S^+$(HNCS). Also appearing in this figure is the best fit obtained with a convoluted linear kernel function (see the text). Note that the data points lie above the fitted curve in the tail region (13.1–13.4 eV).

band (~11.0 eV) and the onset of the third band. Thus, there exist two reasons why the true thermochemical threshold may not be attained.

(i) The rearrangement process may be very slow when there is little excess energy. Isomerization of $HNCS^+$ to $HCNS^+$ may require only about 1.5 eV, but there may be a more substantial barrier to isomerization.

(ii) The density of parent ion states in the relevant energy region (below the onset of the third band) may be very low. As a result, the 0 K threshold deduced from the above treatment, which is equivalent to $\Delta H^\circ_{f_0}$ (HNCS)=25.9 kcal/mol, must be clearly regarded as a lower limit for $\Delta H^\circ_{f_0}$ (HNCS).

*b. $SH^+$ and $NCS^+$ from HNCS.* Figure 7(a) displays the photoion yield curve of $SH^+$(HNCS), and Fig. 7(b), that of $NCS^+$(HNCS). They are strikingly similar, and have onsets near 820 Å≡15.12 eV, the aforementioned adiabatic IP of Eland's fourth band. The threshold domain is probed more sensitively in Figs. 8(a) and 8(b), where convoluted linear kernel functions are compared with the experimental data. The data for $SH^+$ [Fig. 8(a)] are fitted quite well by this function; the 0 K threshold (15.131 eV) is equivalent to $\Delta H^\circ_{f_0}$ (HNCS)=29.6 kcal/mol, when combined with auxiliary data. However, this threshold must also be regarded as an upper limit [and hence the derived $\Delta H^\circ_{f_0}$ (HNCS) as a lower limit] because the formation of $SH^+$ involves rearrangement, it is not the first fragment, and it appears suspiciously at the onset of the fourth photoelectron band. The experimental data for Fig. 8(b) lie above the convoluted linear function in the tail region (14.85–15.05 eV), again implying that the true thermochemical threshold for $NCS^+$ lies lower than the value given by the fitted function, which is 15.061 eV at 0 K. Here, fragment formation involves simple bond cleavage, which is favorable, but the prominent ascent of the $NCS^+$ curve close to the adiabatic IP of the fourth band is still a basis for suspicion.

We note here that the $HCS^+$(HNCS), which has a weak and ill-defined threshold (not shown), also displays a pronounced increase in intensity at ~820 Å.

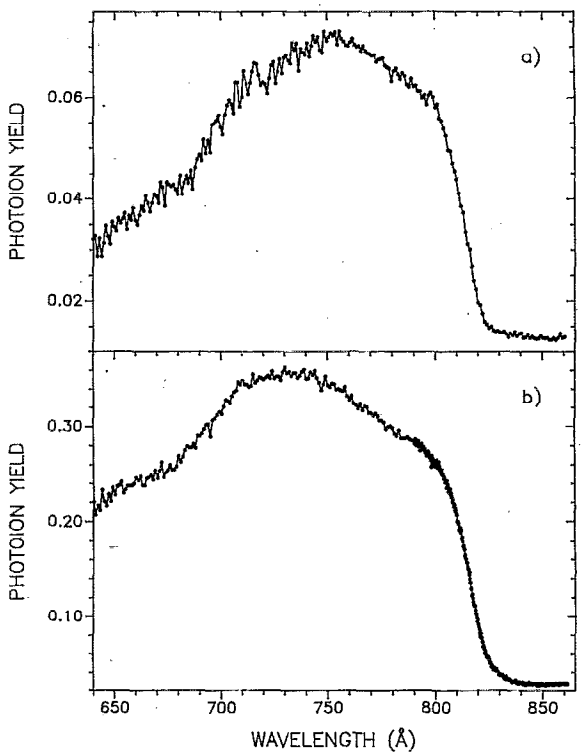


FIG. 7. (a) The photoion yield curve of $SH^+$(HNCS). (b) The photoion yield curve of $NCS^+$(HNCS).

*c. $CS^+$ and $NS^+$ from HNCS.* The photoion yield curves of $CS^+$ and $NS^+$, both weak fragments appearing at higher energy, are shown in Figs. 9(a) and 9(b), respectively. The conspicuous peak in Fig. 9(a) at ~752 Å is almost certainly attributable to a weak impurity of $CO_2$, since that is the strongest autoionizing peak in the spectrum[35] of $CO_2^+(CO_2)$. The corresponding comparisons with convoluted linear kernel functions are displayed in Figs. 10(a) and 10(b). For $CS^+$, the 0 K threshold is 16.884 eV, which is equivalent to $\Delta H^\circ_{f_0}$ (HNCS)≥23.3 kcal/mol. For $NS^+$, the data display more scatter; the 0 K threshold is 16.879 eV, almost the same as for $CS^+$. This coincidence alerts one to the possible presence of a higher energy state of $HNCS^+$, which could conceivably account for both thresholds, but the corresponding band is not apparent in Eland's spectrum. The $NS^+$ threshold implies $\Delta H^\circ_{f_0}$(HNCS)≥27.3±2 kcal/mol. Neither the $CS^+$ nor the $NS^+$ threshold is thermochemically significant, since lower energy thresholds have already established that $\Delta H^\circ_{f_0}$(HNCS)≥29.6 kcal/mol.

*d. More extensive fitting procedures for $S^+$ and $NCS^+$.* The preceding analysis has shown that the convoluted linear kernel function fits the photoion yield curve of $SH^+$(HNCS) quite well, and establishes $\Delta H^\circ_{f_0}$(HNCS) ≥ 29.6kcal/mol. The photoion yield curves of $CS^+$ and $NS^+$ from HNCS are too weak, and occur at too high an energy to provide useful thermochemical threshold values. The photoion yield curves of $S^+$ and $NCS^+$ from HNCS increase sharply at about the

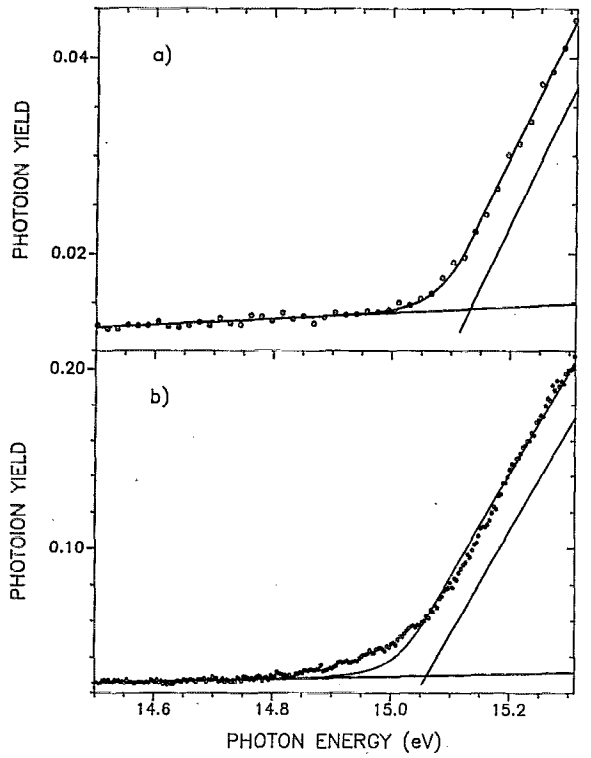


FIG. 8. (a) A magnified view of the threshold region of $SH^+$(HNCS). Note that the convoluted linear kernel function fits the experimental data quite well in this case. (b) A magnified view of the threshold region of $NCS^+$(HNCS). The experimental data points lie above the convoluted linear kernel function in the tail region (14.85–15.05 eV).

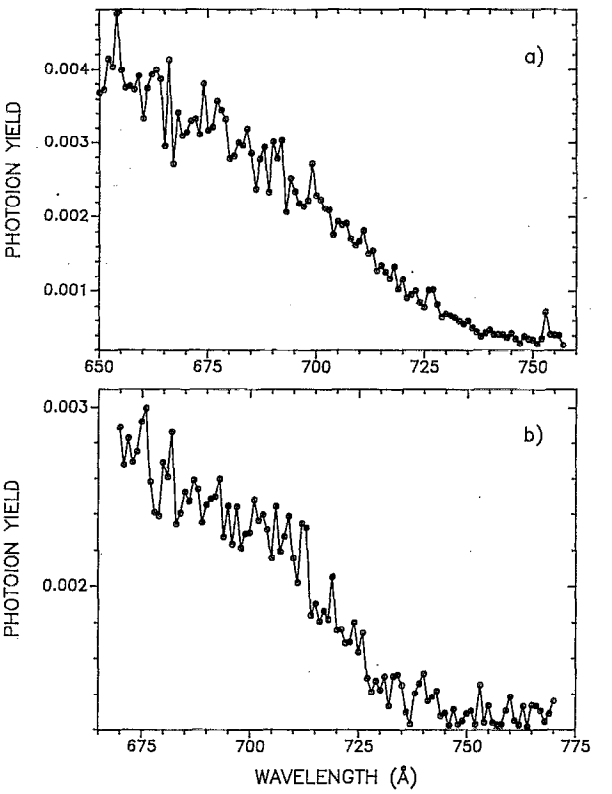


FIG. 9. (a) The photoion yield curve of $CS^+$(HNCS). (b) The photoion yield curve of $NS^+$(HNCS).

onset of the fourth photoelectron band, but below that onset, the data points in each curve lie above the corresponding convoluted linear kernel functions. Our goal here is to attempt a better fit to the data. The approach will be to utilize two convoluted linear functions, one with a shallower slope in the "tail" region, the other similar in nature to the earlier one. The rationale for this approach is as follows.

The probability of formation of a fragment ion at a given internal energy is a product of the probability of formation of the parent ion with that internal energy, and the unimolecular decay rate. We assume that the unimolecular decay rate is a relatively smooth function of the internal energy. However, the energy deposition function may change rather abruptly with photon energy. Consider the excited state of $HNCS^+$ represented by the fourth photoelectron band. There should be one or more Rydberg states of the neutral molecule converging to that limit. The partial oscillator strength density $\Delta f/\Delta E$ of these Rydberg states should smoothly join the differential oscillator strength $df/dE$, at the onset of formation of this excited ionic state. If these Rydberg states all were to autoionize by releasing near zero kinetic energy electrons, then the energy deposition function would also go smoothly through the ionization threshold of the excited state. If, on the other hand, other autoionization mechanisms were to compete, in which lower states of the cation were formed (and concomitantly, higher kinetic energy electrons), then the energy deposition function would be smaller below the ionization onset, and increase more rapidly thereafter.

The simplest implementation of this hypothesis is to use two linear kernel functions, with four floating parameters: two thresholds and two slopes. In Figs. 11(a) and 11(b), the data points for $S^+$(HNCS) and $NCS^+$(HNCS) are fitted to such bilinear convoluted functions. The quality of these fits is much better; the least-squares criterion is improved by a factor 3.2 for $S^+$, and by 7.1 for $NCS^+$, over the single linear convoluted functions. It may be argued that we have introduced two additional variables, and hence the fit should inevitably be improved. However, we have also attempted fits with kernel functions which were power series, and the results were not as good as the bilinear functions.

Another possible criticism is that the tailing is due to collision-induced dissociation, i.e., a bimolecular rather than unimolecular process. Because of the peculiar vaporization behavior of HNCS in its condensed phase, which appears to have several forms, it was not possible to thoroughly test this hypothesis by studying the shape of the photoion yield curve as a function of pressure. However, we have noted that not all fragments display this shallow onset (e.g., $SH^+$ does not), whereas collisional dissociation is probably not as discriminate.

The 0 K thresholds from the shallower slopes of the bilinear convoluted functions are $13.205\pm0.014$ eV for $S^+$, and $14.903\pm0.009$ eV for $NCS^+$. The $S^+$ threshold, combined with auxiliary data, implies $\Delta H^\circ_{f_0}(HNCS) \geqslant 31.0$

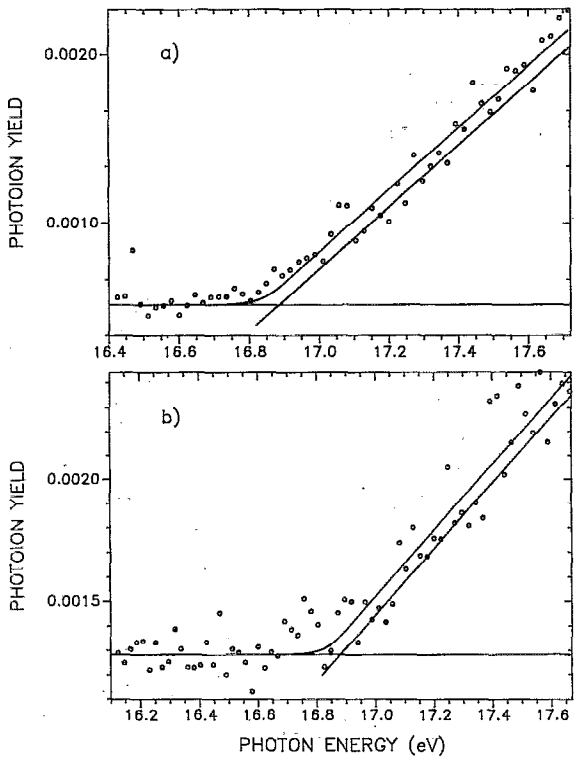


FIG. 10. Magnified views of the threshold regions of (a) $CS^+$ from HNCS and (b) $NS^+$ from HNCS. In each figure, the smooth line represents the best fit to the data of a convoluted linear kernel function.

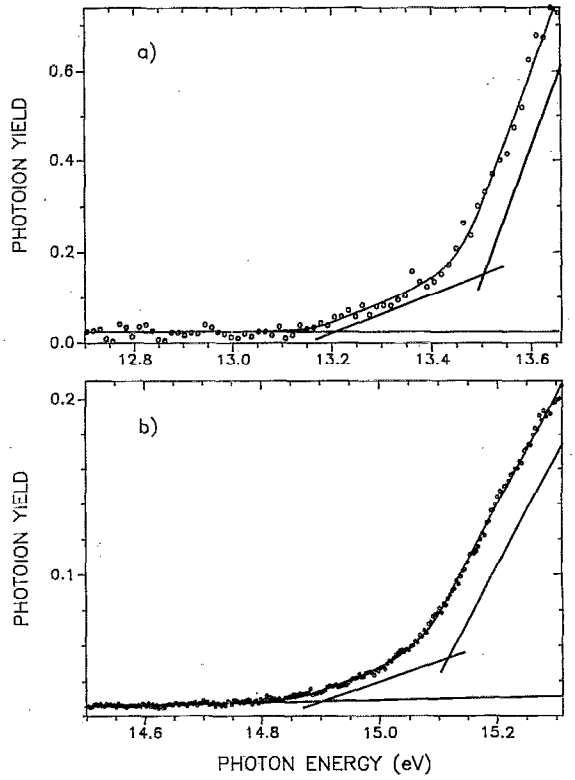


FIG. 11. The threshold regions of (a) $S^+$ from HNCS and (b) $NCS^+$ from HNCS, now fitted with two convoluted linear kernel functions of different slope and threshold. Note that the data points now follow the fitted curves quite well, as borne out by the least-squares criterion.

kcal/mol. The $NCS^+$ threshold will be used (*vide infra*) to deduce an upper limit to $D_0$(H–NCS).

## B. Photoionization of NCS

An overview of the photoion yield curve of $NCS^+$(NCS), obtained upon hydrogen abstraction of HNCS by atomic fluorine, appears in Fig. 12. The spectrum has numerous strong autoionizing features, whose interpretation we defer (*vide infra*).

### 1. The threshold region of $NCS^+$(NCS)

A magnified view of the threshold region is shown in Fig. 13. There is a region of initial ascent, between ~1165–1159 Å, followed by a plateau between ~1159–1153 Å. The initial ascent region can itself be described as a shallow slope (~1165–1161.5 Å) followed by a steeper slope (~1165–1161.5 Å). We interpret the shallow slope as photoionization from a low-lying excited state of NCS, and the steeper slope as photoionization from NCS in its ground state.

Northrup and Sears[36] have studied the electronic spectrum of NCS by laser-induced fluorescence. They established that the ground state is $X\ ^2\Pi_{3/2}$, with the excited spin–orbit component $^2\Pi_{1/2}$ lying 322.90 $cm^{-1}$ to higher energy. Two additional Renner–Teller split states are found at 364.44 and 375.1 $cm^{-1}$, as well as still higher states which are not of current interest. The energy difference (322.90 $cm^{-1}$) between $X\ ^2\Pi_{1/2}$ and $^2\Pi_{3/2}$ amounts to ~4.4 Å in the region around 1165 Å. This is almost exactly the difference between the half-rise of a first step (~1164.5 Å) and the half-rise point of the steeper slope (1159.9 Å). The Boltzmann abundance of a state excited by 322.90 $cm^{-1}$ at room temperature is about 20%. This is approximately the ratio of the first step height to that of the plateau region. These observations sup-

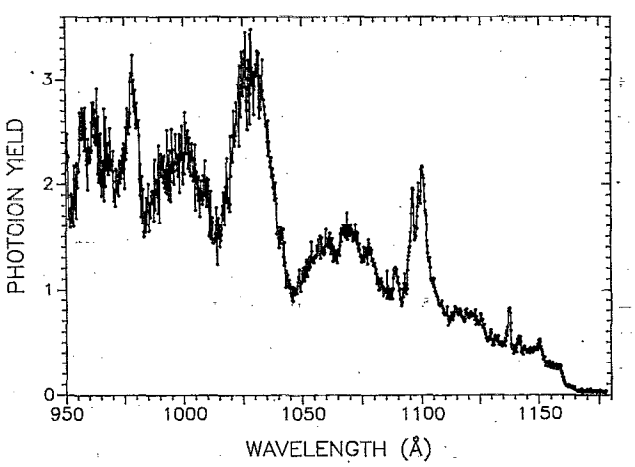


FIG. 12. An overview of the photoion yield curve of $NCS^+$(NCS). The NCS is prepared *in situ* by the reaction of F atoms with HNCS.

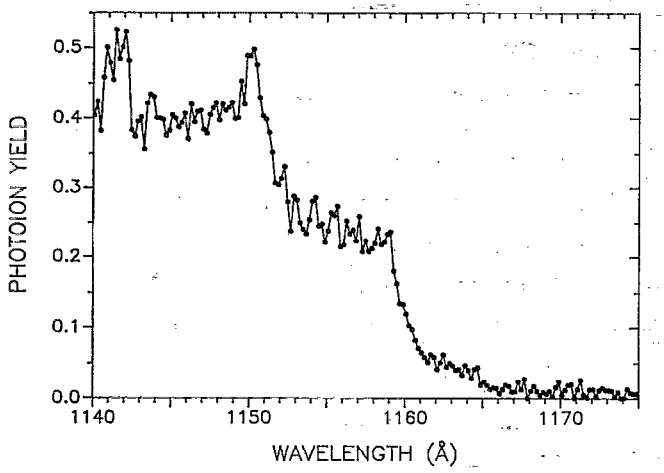


FIG. 13. A magnified view of the threshold region of $NCS^+$ from NCS. The first onset of signal above background, at ~1165 Å, is attributed to ionization from the Boltzmann populated $^2\Pi_{1/2}$ state, whereas the steeper ascent (half-rise at 1159.9 Å) is identified with the adiabatic IP, forming $NCS^+$, $^2\Pi_{3/2}$.

port the conclusion that the adiabatic IP of NCS, $X\ ^2\Pi_{3/2}$, is 1159.9±0.5 Å≡10.689±0.005 eV, and that the weak ionization detected at lower energy is attributable to the thermally populated NCS, $^2\Pi_{1/2}$. By analogy with $NCO^+$, we tentatively identify the ground state of $NCS^+$ as $^3\Sigma^-$.

### 2. Interpretation of the autoionizing features

The prominent autoionizing features of the $NCS^+$(NCS) spectrum are listed in Table IV. In the absence of a photoelectron spectrum and with no clearly visible Rydberg progressions, the interpretation given here must be regarded as highly speculative.

(a) Rather sharp peaks can be noted at 10.90, 11.27, and 11.31 eV. The 10.90 and 11.27 eV peaks could be successive members of a Rydberg series, with $n^*=3.74$ and 4.74, respectively, converging to an IP of $11.87_5$ eV. The antecedent would be at ~1232 Å, which is below threshold, and the successor would be at 1082 Å, where no obvious peak exists. If we take the combination of 10.90 and 11.31 eV, we determine an IP of $11.95_7$ eV, with $n^*=3.59$ and 4.59. The antecedent would again occur below the first IP, at ~1248 Å, and the successor at 1076 Å. The closest peak to either successor is the sharp peak at ~1089 Å. We tentatively suggest that there may be a sharp peak in the photoelectron spectrum at ~11.9 eV.

(b) It is tempting to relate the two most intense features at 12.06 and 12.67 eV, on the one hand, and the broader, less intense features centered at ~11.59 and ~12.42 eV on the other. The first couplet would suggest an IP of $\sim 13.48_8$ eV, with $n^*$ values of 3.08 and 4.08. The antecedent would occur at λ=1198 Å (below threshold) and the successor at ~957 Å, where a peak does exist. The broader couplet can be related to an IP of $\sim 13.39_0$ eV, with $n^*=2.75$ and 3.75, respectively. The succeeding member of such a series should occur at ~970 Å. The closest peak in this region is at ~968 Å. Our tentative suggestion is that one or two photoelectron bands may be observable in the vicinity of 13.5 eV.

TABLE IV. Wavelengths of the prominent autoionization peaks appearing in the photoion yield curve of $NCS^+$(NCS). b=broad; vb=very broad.

| λ (Å) | $E$ (eV) |
|---|---|
| 1150.2±0.5 | 10.779±0.005 |
| 1141.3±0.5 | 10.863±0.005 |
| 1137.2±0.5 | 10.903±0.005 |
| 1100.1±0.5 | 11.270±0.005 |
| 1098.6±0.5 | 11.286±0.005 |
| 1096.0±0.5 | 11.312±0.005 |
| 1088.9±0.7 | 11.386±0.007 |
| 1078.0±1.0 b | $11.50_1$ ±0.01 |
| 1069.5±1.0 b | $11.59_3$ ±0.01 |
| 1060.0±1.0 b | $11.69_7$ ±0.01 |
| 1028.5±1.0 vb | $12.05_5$ ±0.01 |
| 998.0±1.0 vb | $12.42_3$ ±0.01 |
| 978.5±1.0 b | $12.67_1$ ±0.01 |
| 968.0±1.0 b | $12.80_8$ ±0.01 |
| 962.5±1.0 b | $12.88_1$ ±0.01 |
| 957.0±1.0 b | $12.95_6$ ±0.01 |

### C. Photodissociative ionization of NCS–SCN

Our experimental observation of the reaction of $Cl_2$ with AgSCN was similar to that described by Frost *et al.*[24] If there is any moisture or HCl present in the inlet system, HCNS is observed. When the system is dry, $(NCS)_2$ grows in, but it is difficult to maintain a steady state of evolution. As the abundance of $(NCS)_2$ declines, ClSCN appears, and remains for an extended period. Consequently, we were unable to find conditions where only $(NCS)_2$ was generated for an extended period, and in a steady state. In order to derive the desired spectrum of $NCS^+$ from thiocyanogen, two types of experiments were performed.

(1) A scan was taken in the early part of the run, before ClSCN began to appear. At this time, the intensity of $NCS^+[(NCS)_2]$ was weak. To enhance this signal, the bandwidth of the mass spectrometer was increased. With poorer mass resolution, some $HNCS^+$ ($m/e=59$) was incorporated into the $NCS^+$ ($m/e=58$) signal. In the analysis of this data set, the $HNCS^+$ contribution was subtracted by making use of the previously determined photoion yield curve of $HNCS^+$(HNCS), as given in Fig. 3.

(2) As the $NCS^+$ signal from $(NCS)_2$ increased, the mass resolution could be improved, thereby rejecting $HNCS^+$. However, toward the end of this run, a small amount of ClSCN began to appear. The appearance potential of $NCS^+$ from ClSCN is lower than that of $NCS^+$ from $(NCS)_2$. This was established by examining $NCS^+$(ClSCN) at a still later part of the run, when thiocyanogen had ceased to appear, and only ClSCN was being evolved. With this information, and a measure of the growth curve of ClSCN, it was possible to subtract the contribution of ClSCN to the $NCS^+$ curve.

Both data sets, with their respective corrections, gave essentially the same shape of the photoion yield curve of

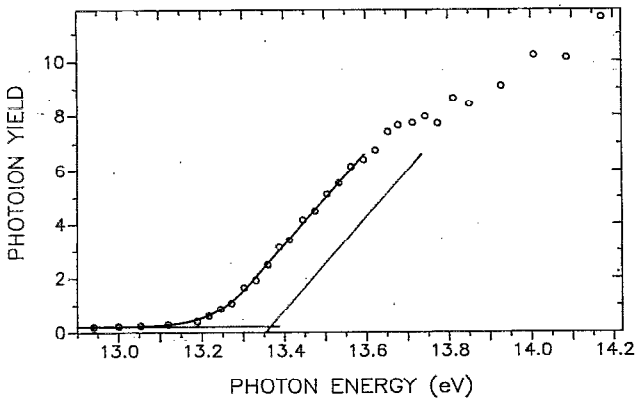


FIG. 14. The photoion yield curve of $NCS^+$(NCS–SCN). The smooth curve is the best fit of a linear kernel function convoluted with a thermal broadening function, described in the text and Appendix.

$NCS^+$ from $(NCS)_2$, and the same threshold. The result of the experiment described in (2) above is shown in Fig. 14. The smooth curve is the best fit of a linear kernel function convoluted with a broadening function having the form a $\epsilon^3 e^{-\epsilon/kT}$, with $T=408$ K. This broadening function is a numerical fit to the more complex Haarhoff function (see the Appendix). In this case, the result is essentially the same as would be obtained by a linear extrapolation of the threshold region of the curve in Fig. 14, shifted by the average internal energy. With a linearly extrapolated threshold of 937.5±1.0 Å≡13.225±0.014 eV, and an internal energy correction of 0.141 eV, one arrives at a 0 K threshold of 13.366±0.014 eV.

## IV. INTERPRETATION OF RESULTS

### A. Adiabatic ionization potentials

#### 1. $HNCS^+$(HNCS)

The linear onset of $HNCS^+$(HNCS) leads to IP(HNCS)≤9.92 eV. The gradual increase implies a significant change in geometry between HNCS and the ground state of $HNCS^+$.

#### 2. $NCS^+$(NCS)

After taking into account the contribution of the low-lying $^2\Pi_{1/2}$ excited state of NCS on the photoion yield curve, the adiabatic ionization potential of NCS, $X\ ^2\Pi_{3/2}$ is found to be 1159.9±0.5 Å≡10.689±0.005 eV. The onset is relatively abrupt, implying that a major structural change does not occur. However, a short vibrational progression with a frequency of ~630 $cm^{-1}$ could be inferred from step-like features near threshold. Such a frequency is reasonably close to $\nu_3=735.4$ $cm^{-1}$ found by Northrup and Sears[36] for NCS neutral. According to Jacox,[37] this frequency can roughly be characterized as a C–S stretch, with the C–N stretch being 1942 $cm^{-1}$ and the bend, 387 $cm^{-1}$ (375.96 $cm^{-1}$ from Northrup and Sears). Hence, this simple picture implies an increase in the C–S distance in $NCS^+$, compared to that in NCS.

### B. Thermochemical inferences

#### 1. $\Delta H_f^\circ$(HNCS)

A rigorous lower limit to $\Delta H_f^\circ$(HNCS) can be obtained from a satisfactory fit of a convoluted linear kernel function to the photoion yield curve of $SH^+$, i.e.,

$$HNCS+h\nu\rightarrow SH^++CN+e,\quad \Delta H_0\leqslant 15.131\ \text{eV}.$$

By utilizing $\Delta H_{f_0}^\circ(SH) = 34.07 \pm 0.72$ kcal/mol,[38] IP(SH)=10.4212±0.0004 eV,[39] and $\Delta H_{f_0}^\circ(CN) = 104.1 \pm 0.5$ kcal/mol,[40] we can deduce $\Delta H_{f_0}^\circ(HNCS) \geqslant 29.6 \pm 0.9$ kcal/mol.

A somewhat less rigorous, but in our judgment a quite likely upper limit results from the bilinear convoluted fit to the $S^+$ photoion yield curve:

$$HNCS+h\nu\rightarrow S^++HCN+e,\quad \Delta H_0\leqslant 13.205\ \text{eV}.$$

Together with $\Delta H_{f_0}^\circ(S) = 65.71 \pm 0.04$ kcal/mol,[41] IP(S) =10.360 eV,[42] and $\Delta H_{f_0}^\circ(HCN) = 30.9 \pm 0.6$ kcal/mol[43] this enables one to infer $\Delta H_{f_0}^\circ(HNCS) \geqslant 31.0 \pm 0.7$ kcal/mol, and $\Delta H_{f298}^\circ(HNCS) \geqslant 30.4 \pm 0.7$ kcal/mol.

#### 2. $\Delta H_f^\circ$(NCS)

There are two independent sources of data for this quantity.

(a) From the appearance potential of $NCS^+$(HNCS) and the measured IP(NCS). Thus,

$$HNCS+h\nu\rightarrow NCS^++H+e,\quad \Delta H_0\leqslant 14.903\pm 0.009\ \text{eV},$$

$$e+NCS^+\leftarrow NCS,\quad \Delta H_0=-10.689\pm 0.005\ \text{eV},$$

$$HNCS\rightarrow NCS+H,\quad \Delta H_0\leqslant 4.214\pm 0.010\ \text{eV}.$$

With $\Delta H_{f_0}^\circ(HNCS) \geqslant 31.0 \pm 0.7$ kcal/mol, and $\Delta H_{f_0}^\circ(H) = 51.633$ kcal/mol, we infer $\Delta H_{f_0}^\circ(NCS) \cong 76.5$ kcal/mol.

(b) From the appearance potential of $NCS^+[(NCS)_2]$ and $\Delta H_f^\circ[(NCS)_2]$, together with IP(NCS):

$$(NCS)_2+h\nu\rightarrow NCS^++NCS+e,\quad \Delta H_0\leqslant 13.366\pm 0.014\ \text{eV},$$

$$e+NCS^+\leftarrow NCS,\quad \Delta H_0=-10.689\pm 0.050\ \text{eV},$$

$$(NCS)_2\rightarrow 2NCS,\quad \Delta H_0\leqslant 2.677\pm 0.015\ \text{eV}.$$

The heat of formation of $(NCS)_2$ is given as 82.3±1.8 kcal/mol by Vanderzee and Quist[44] and 83.7±1.5 kcal/mol by Pedley and Rylance.[45] The latter incorporates some changes in the heats of formation of the components entering into the measurements performed earlier by Vanderzee and Quist. These heats of formation refer to 298 K, but there is almost no change in going to 0 K. The Vanderzee value implies $\Delta H_{f_0}^\circ(NCS) \leqslant 72.0 \pm 1.0$ kcal/mol, while the Pedley value yields $\Delta H_{f_0}^\circ(NCS) \leqslant 72.7 \pm 0.8$ kcal/mol.

Since the measurement described in (b) leads to an upper limit to $\Delta H_f^\circ(NCS)$ which is lower than the value obtained in (a), it must take precedence. Thus, we conclude that

$\Delta H^\circ_{f_0}$(NCS)$\leqslant$72.7$\pm$0.8 kcal/mol, $\Delta H^\circ_{f298}$(NCS)$\leqslant$73.1$\pm$0.8 kcal/mol, and that the $NCS^+$ appearance potential from HNCS is retarded by about 4 kcal/mol.

### 3. $\Delta H^\circ_{f_0}(NCS^+)$

From the value found in Sec. IV B 2, and IP(NCS) $=10.689\pm0.005$ eV, we obtain $\Delta H^\circ_{f_0}(NCS^+) \leqslant 319.2 \pm 0.9$ kcal/mol.

### 4. $D_0$(H–NCS)

Utilizing $\Delta H^\circ_{f_0}(HNCS)\geqslant 31.0\pm0.7$ kcal/mol, $\Delta H^\circ_{f_0}(NCS)\leqslant 72.7\pm0.8$ kcal/mol, and $\Delta H^\circ_{f_0}(H)=51.633$ kcal/mol, we deduce $D_0$(H–NCS)$\leqslant$93.3$\pm$1.1 kcal/mol. This is preferred over the direct measurements of $NCS^+$ from HNCS which, together with the IP of NCS, yields $D_0$(H–NCS)$\leqslant$97.2$\pm$0.2 kcal/mol.

### 5. $\Delta H^\circ_f$ ($HNCS^+$), PA(NCS)

The inherent nature of impact methods leads to upper and lower limits. When these are combined, the results can sometimes not be clearly determined as upper or lower limits, and hence can only be approximate. Thus

$$\Delta H^\circ_{f_0}(HNCS^+)=(\geqslant 31.0\pm0.7 \text{ kcal/mol}) + (\leqslant 228.8 \text{ kcal/mol}),$$

where the second item on the right-hand side is IP(HNCS). Thus,

$$\Delta H^\circ_{f_0}(HNCS^+)\cong 259.8 \text{ kcal/mol}$$

and

$$\Delta H^\circ_{f_{298}}(HNCS^+)\cong 259.2 \text{ kcal/mol}.$$

With $\Delta H^\circ_{f298}(H^+) = 365.7$ kcal/mol and $\Delta H^\circ_{f298}(NCS) \leqslant 73.1 \pm 0.8$ kcal/mol, the proton affinity of NCS is ~179.6 kcal/mol.

## V. DISCUSSION

The value of the adiabatic ionization potential of HNCS obtained in the present study ($\leqslant$9.92 eV) is not very different from earlier values inferred from He I photoelectron spectroscopy: 10.05$\pm$0.1,[24] 9.94$\pm$0.02 eV.[25] However, the earlier results implied a more-or-less abrupt onset of ionization, which is associated with a small geometrical change between the neutral species and its cation, whereas the very gradual onset currently observed is consistent with a change from a bent neutral to a linear cation. The neutral HNCS is known to be bent, the linear cation structure is the result of a concurrent *ab initio* calculation.[29]

The value of the H–NCS bond energy deduced in the present study [$D_0$ (H–NCS)$\leqslant$93.3$\pm$1.1 kcal/mol, $D_{298}$ (H–NCS)$\leqslant$94.8$\pm$1.1 kcal/mol, is in satisfactory agreement with $D_{298}$(H–NCS)=96$\pm$6 kcal/mol inferred[18] from a combination of gas phase acidity and the electron affinity of NCS, and departs significantly from the value 111$\pm$1 kcal/mol listed by Lias *et al.*[8] Our current value is about 17 kcal/mol lower than $D_0$ (H–NCO)$\leqslant$110.1$\pm$0.3 kcal/mol recently reported by us.[1]

The heat of formation of HNCS deduced currently [$\Delta H^\circ_{f_0}$(HNCS) > 29.6 kcal/mol, and very likely $\geqslant$31.0 $\pm$0.7 kcal/mol; $\Delta H^\circ_{f298}$(HNCS) > 29.0 kcal/mol, and very likely $\geqslant$30.4$\pm$0.7 kcal/mol] is in surprisingly good agreement with the value in the NBS compilation,[9] $\Delta H^\circ_{f298}$(HNCS) = 30.5 $\pm$ 1.5 kcal/mol, based upon a heat of solution measured in 1882, and a heat of vaporization appearing only in a Ph.D. thesis. It differs from the value $\Delta H^\circ_f$(HNCS) $\leqslant$ 27.3 $\pm$ 0.7 kcal/mol which can be inferred from the onset of CS fluorescence upon ultraviolet photodissociation of HNCS.

The heat of formation of NCS obtained in this study [$\Delta H^\circ_{f_0}$(NCS)$\leqslant$72.7$\pm$0.8 kcal/mol; $\Delta H^\circ_{f_{298}}$(NCS)$\leqslant$73.1$\pm$0.8 kcal/mol] is below the range [$\Delta H^\circ_{f_0}$(NCS)=74.2–79.7 kcal/mol] deduced by us from the photodissociation thresholds of $CH_3NCS$ and $CH_3SCN$ obtained by D'Amario *et al.*[20] and Tokue *et al.*[22]

In summary, the present experiments have provided thermochemical data which provide modern support of an old value of $\Delta H^\circ_f$(HNCS). However, both $D_0$(H–NCS) and $\Delta H°$(NCS) are found to be lower than prior literature values.

## VI. CONCLUSIONS

(1) The adiabatic ionization potential of HNCS is found to be $\leqslant$9.92 eV by photoionization mass spectrometry. The shape of the photoion yield curve near threshold implies a marked change in geometry upon ionization, presumably to a linear $HNCS^+$ structure.

(2) The adiabatic ionization potential of NCS, $X\ ^2\Pi_{3/2}$ is measured to be 10.689$\pm$0.005 eV.

(3) The appearance potentials of two different fragments lead to $\Delta H^\circ_{f_0}$(HNCS) > 29.6 kcal/mol, and very likely $\geqslant$31.0$\pm$0.7 kcal/mol.

(4) The derived value of $D_0$(H–NCS) is $\leqslant$93.3$\pm$1.1 kcal/mol.

(5) The heat of formation of NCS is found to be $\leqslant$72.7 $\pm$0.8 (0 K) and $\leqslant$73.1$\pm$0.8 kcal/mol (298 K), based upon the appearance potential of $NCS^+$ from NCS–SCN. Consequently, $\Delta H^\circ_{f_0}(NCS^+) \leqslant 319.2 \pm 0.9$ kcal/mol.

(6) The following approximate values are inferred: $\Delta H^\circ_{f_0}(HNCS^+) \cong 259.8$ kcal/mol; PA(NCS)$\cong$179.6 kcal/mol.

(7) A method for determining appearance potentials by a more objective procedure is described, and implemented.

(8) Autoionizing structure is observed in the photoion yield curves of $HNCS^+$ (HNCS) and $NCS^+$(NCS). An analysis is offered for the former, based upon the He I photoelectron spectrum. Since no photoelectron spectrum of NCS exists, the analysis attempted in this case is unavoidably more speculative.

## ACKNOWLEDGMENTS

This work was performed under the auspices of the Office of Basic Energy Sciences, U.S. Department of Energy, under Contract No. W-31-109-ENG-38.

## APPENDIX

We wish to find an expression for $\rho$ in the internal energy distribution function

$$P(E)=\rho\, e^{-E/kT},$$

where $\rho$ includes vibrations and rotations.

A general expression is given by Haarhoff,[34] p. 106,

$$\rho_{vr}(E_{vr})=\frac{Z_0(\Pi_k G_k)^{1/2} I_{q/2}(\epsilon_{vr})}{h^q}.$$

Here, $Z_0$ is a number, $q$ is the number of rotations (generally 3 for polyatomics, although internal rotations can be accommodated), $G_k$ are moments of inertia [and therefore, for a particular molecule, $(G_1G_2G_3)^{1/2}$ is just a number], $h^q$ is also a constant, and hence the entire energy dependence resides in $I_{q/2}$. On p. 105, he gives an expression for $I_{q/2}$, which we use for the case of HNCS, $q/2=3/2$ below:

$$I_{3/2}=\left\{\left(\frac{1}{3\pi}\right)^{1/2}\left(\frac{6}{7.5}\right)^{7}\left(1-\frac{1}{12(7.5)}\right)\frac{\lambda(h\nu)^{-1/2}}{(1+\epsilon/\epsilon_z)}\right\}\times\left[\left(1+\frac{\epsilon}{2\epsilon_z}\right)\left(1+\frac{2\epsilon_z}{\epsilon}\right)^{(\epsilon/2\epsilon_z)^{15/2}}\right]\times\left[1-\frac{1}{(1+\epsilon/\epsilon_z)^2}\right]^{\beta_m},$$

where the expression for $\beta_m$ is given on p. 104:

$$\beta_m=\left(6+\frac{3}{2}-1\right)\left(6+\frac{3}{2}-2\right)\frac{\overline{\nu^2}}{(\bar{\nu})^2}-6\left(6+\frac{3}{2}\right)\Big/6\times6$$
$$=0.432\ 079.$$

The frequencies given by Draper and Werner[46] are used to evaluate

$$\frac{\overline{\nu^2}}{(\bar{\nu})^2}=1.6938.$$

Also, $1/\lambda=\Pi_i(\nu_i/\bar{\nu})=(\overline{\nu_{\text{geom}}}/\overline{\nu_{\text{arithm}}})^6=0.1659$ or $\lambda=6.0272$. If we express the energy $\epsilon$ in units of $\epsilon_z$, the zero point energy, we finally arrive at

$$I_{3/2}=\frac{0.407\ 1544/\sqrt{3}}{(1+\epsilon)}\left[\left(1+\frac{\epsilon}{2}\right)\left(1+\frac{2}{\epsilon}\right)^{\epsilon/2}\right]^{15/2}\times\left[1-\frac{1}{(1+\epsilon)^2}\right]0.432\ 079.$$

For subsequent fitting to the experimental data, it is convenient to utilize a simpler function of the form

$$P(E)=\text{const}\ E\, e^{-E/kT},$$

which has been fitted numerically to the more cumbersome Haarhoff function. The quality of this fit is demonstrated in Fig. 4. Here, $T$ has the artificial value of 373.5 K.

For the case of $(NCS)_2$, we utilize the frequencies given by Jensen *et al.*[47] With 12 vibrational frequencies, we obtain

$$I_{3/2}=\frac{\text{const}}{(1+\epsilon)}\left[\left(1+\frac{\epsilon}{2}\right)\left(1+\frac{2}{\epsilon}\right)^{\epsilon/2}\right]^{13.5}\times\left[1-\frac{1}{(1+\epsilon)^2}\right]1.778\ 7555.$$

With 11 vibrational frequencies and one internal rotor (torsion), the expression is

$$I_{4/2}=\frac{\text{const}}{(1+\epsilon)}\left[\left(1+\frac{\epsilon}{2}\right)\left(1+\frac{2}{\epsilon}\right)^{\epsilon/2}\right]^{13}\times\left[1-\frac{1}{(1+\epsilon)^2}\right]1.600\ 8467.$$

Both expressions can be numerically fitted with the simpler function

$$P(E)=\text{const}\ E^3\, e^{-E/kT},$$

with $T$ having the artificial values of 426 and 408 K, respectively.

[1] See B. Ruscic and J. Berkowitz, J. Chem. Phys. **100**, 4498 (1994).
[2] E. Borisov, A. M. Mebel', B. A. Knyazev, V. B. Zabrodin, and A. A. Korkin, Bull. Acad. Sci. Russia, Chem. Ser. No. 7, p. 1222 (1992), Engl. transl.
[3] N. Pinnavaia, M. J. Bramley, M.-D. Su, W. H. Green, and N. C. Handy, Mol. Phys. **78**, 319 (1993).
[4] A. L. L. East, C. S. Johnson, and W. D. Allen, J. Chem. Phys. **98**, 1299 (1993).
[5] A. L. L. East and W. D. Allen, J. Chem. Phys. **99**, 4638 (1993).
[6] B. B. Back, J. J. Christiansen, O. J. Nielsen, and H. Svanholt, Acta Chem. Scand. Sect. A **31**, 666 (1977).
[7] T. A. Spiglanin, R. A. Perry, and D. W. Chandler, J. Phys. Chem. **90**, 6184 (1986); T. A. Spiglanin and D. W. Chandler, Chem. Phys. Lett. **141**, 428 (1987).
[8] S. G. Lias, J. E. Bartmess, J. F. Liebman, J. L. Holmes, R. D. Levin, and W. G. Mallard, J. Phys. Chem. Ref. Data **17**, Suppl. No. 1 (1988).
[9] D. D. Wagman, W. H. Evans, V. B. Parker, R. H. Schumm, I. Halow, S. M. Bailey, K. L. Churney, and R. L. Nuttall, J. Phys. Chem. Ref. Data **11**, Suppl. No. 2 (1982).
[10] E. Domalski, NIST (private communication).
[11] A. Joannis, Ann. Chim. Phys. Ser. 5 **26**, 534 (1882).
[12] J. T. Brandenburg, Ph.D. thesis, University of Nebraska, Lincoln, Nebraska (1958).
[13] M. Lenzi, A. Mele, and M. Paci, Gazz. Chim. Ital. **103**, 977 (1973).
[14] Reference 13 gives 10.21 eV for the photon energy at H Lyman-$\alpha$.
[15] S. T. Gibson, J. P. Greene, and J. Berkowitz, J. Chem. Phys. **83**, 4319 (1985) give $\Delta H^{\circ}_{f_0}(NH^+)=396.3\pm0.3$ kcal/mol. E. de Beer, M. Born, C. A. de Lange, and N. C. Westwood, Chem. Phys. Lett. **186**, 40 (1991) report IP(NH)=13.476±0.002 eV. Combined, they yield $\Delta H^{\circ}_{f_0}(NH)=85.5\pm0.3$ kcal/mol.
[16] The value $\Delta H^{\circ}_{f_0}(CS)=65.8\pm0.6$ kcal/mol is an average of the values given by *P.* Coppens, J. C. Reynaert, and J. Drowart, J. Chem. Soc. Faraday Trans. 2, **75**, 292 (1979); J. H. D. Eland and J. Berkowitz, J. Chem. Phys. **70**, 5151 (1979).
[17] K. P. Huber and G. Herzberg, *Molecular Spectra and Molecular Structure. IV. Constants of Diatomic Molecules* (Van Nostrand Reinhold, New York, 1979).
[18] S. E. Bradforth, E. H. Kim, D. W. Arnold, and D. M. Neumark, J. Chem. Phys. **98**, 800 (1993).
[19] V. M. Bierbaum, J. J. Grabowski, and C. H. DePuy, J. Phys. Chem. **88**, 1389 (1984) found that $NCS^-$ does not react with

$CF_2HCOOH$($\Delta G_{acid}$=324 kcal/mol) but does react with HBr($\Delta G_{acid}$=318 kcal/mol). Lias *et al.* (Ref. 8) apparently took the mean of these values to arrive at $\Delta G_{acid}$(HNCS)=321 kcal/mol, with a generous ±5 kcal/mol error limit. The difference between their listed $\Delta H_{acid}$(HNCS) and $\Delta G_{acid}$(HNCS)≅8 kcal/mol suggests that they used a generic value for $T\Delta S$. We have explicitly calculated $S^\circ_{298}(NCS^-)$=55.65 cal/deg mol from vibrational frequencies and a rotational constant given in Ref. 18. Similarly, we obtain $S^\circ_{298}$(HNCS)=60.30 cal/deg mol from rotational constants given by Yamada *et al.* (Ref. 27) and vibrational frequencies given by Draper and Werner (Ref. 46). Together with $S^\circ_{298}(H^+)$=26.01 cal/deg mol, this gives $T\Delta S$=6.37 kcal/mol, or $\Delta H_{acid}$(HNCS)=321+6.4=327.4 kcal/mol. Then, taking EA(NCS)=3.537±0.005 eV from Ref. 18 and IP(H)=13.5984 eV, we arrive at $D_{298}$(H–NCS)=95.4 kcal/mol, and we retain the ±5 kcal/mol error limit.

[20] P. D'Amario, G. Di Stefano, M. Lenzi, and A. Mele, J. Chem. Soc. Faraday Trans. 1 **68**, 940 (1972).

[21] F. J. Northrup and T. J. Sears, J. Chem. Phys. **91**, 762 (1989).

[22] I. Tokue, A. Hiraya, and K. Shobatake, Chem. Phys. **117**, 315 (1987).

[23] B. Ruscic, J. P. Greene, and J. Berkowitz, J. Phys. B **17**, 1503 (1984); B. Ruscic and J. Berkowitz, Phys. Rev. Lett. **50**, 675 (1983).

[24] D. C. Frost, C. Kirby, W. M. Lau, C. B. MacDonald, C. A. McDowell, and N. P. C. Westwood, Chem. Phys. Lett. **69**, 1 (1980).

[25] J. H. D. Eland, Philos. Trans. R. Soc. London Ser. A **268**, 87 (1970).

[26] S. Cradock, E. A. Ebsworth, and J. D. Murdoch, J. Chem. Soc. Faraday Trans. 2 **68**, 86 (1972).

[27] K. Yamada, M. Winnewisser, G. Winnewisser, L. B. Szalanski, and M. C. L. Gerry, J. Mol. Spectrosc. **79**, 295 (1980).

[28] H. Leung, R. J. Suffolk, and J. D. Watts, Chem. Phys. **109**, 289 (1986).

[29] L. A. Curtiss (private communication).

[30] K. A. Peterson, R. C. Mayrhofer, and R. C. Woods, J. Chem. Phys. **93**, 4946 (1990).

[31] J. B. Burkholder, A. Sinha, P. D. Hammer, and C. J. Howard, J. Mol. Spectrosc. **126**, 72 (1987).

[32] P. M. Guyon and J. Berkowitz, J. Chem. Phys. **54**, 1814 (1971).

[33] B. Ruscic and J. Berkowitz, J. Phys. Chem. **97**, 11,451 (1993).

[34] P. C. Haarhoff, Mol. Phys. **7**, 101 (1963).

[35] J. Berkowitz, *Photoabsorption, Photoionization, and Photoelectron Spectroscopy* (Academic, New York, 1979), p. 251.

[36] F. J. Northrup and T. J. Sears, Mol. Phys. **71**, 45 (1990).

[37] M. E. Jacox, J. Phys. Chem. Ref. Data **19**, 1412 (1990).

[38] J. M. Nicovich, K. D. Kreutter, C. A. van Dijk, and P. H. Wine, J. Phys. Chem. **96**, 2518 (1992).

[39] C.-W. Hsu, B. P. Baldwin, C.-L. Liao, and C. Y. Ng, J. Chem. Phys. **100**, 8047 (1994).

[40] Y. Huang, S. A. Barts, and J. B. Halpern, J. Phys. Chem. **96**, 425 (1992).

[41] L. V. Gurvich, I. V. Veyts, and C. B. Alcock, *Thermodynamic Properties of Individual Substances*, 4th ed. (Hemisphere, New York, 1989), Vol. I.

[42] V. Kaufman, Phys. Scr. **26**, 439 (1982).

[43] This quantity, $\Delta H^\circ_{f_0}$(HCN) = 30.9 ± 0.6 kcal/mol, is obtained by combining $\Delta H^\circ_{f_0}$(CN) from Ref. 35 with an average value of $D_0$(H–CN) of 124.8±0.4 kcal/mol, based on $D_0$(H–CN) of 124.6±0.2 kcal/mol [J. Berkowitz, W. A. Chupka, and T. A. Walter, J. Chem. Phys. **50**, 1497 (1969)] and $D_0$(H–CN) of 125.06±0.43 kcal/mol [G. P. Morley, I. R. Lambert, M. N. R. Ashfold, K. N. Rosser, and C. M. Western, J. Chem. Phys. **97**, 3157 (1992)]. This value is more precise than that given in standard compilations.

[44] C. E. Vanderzee and A. S. Quist, Inorg. Chem. **5**, 1238 (1966).

[45] J. B. Pedley and J. Rylance, "Sussex—N. P. L. Computer Analyzed Thermochemical Data: Organic and Organometallic Compounds," University of Sussex (1977). The value given there is taken from J. D. Cox and G. Pilcher, *Thermochemistry of Organic and Organometallic Compounds* (Academic, London, 1970).

[46] G. R. Draper and R. L. Werner, J. Mol. Spectrosc. **50**, 369 (1974).

[47] N. H. Jensen, R. Wilbrandt, P. Pagsberg, R. E. Hester, and E. Ernstbrunner, J. Chem. Phys. **71**, 3326 (1979).